AGU PUBLICATIONS

Geophysical Research Letters

RESEARCH LETTER
10.1002/2016GL070654

Key Points:
- In situ reservoir condition micro-CT imaging of coal flooded by supercritical CO_2
- Microcleat closure due to supercritical CO_2 injection
- Internal swelling stress induced fracturing of the mineral phase (inside the coal)

Supporting Information:
- Supporting Information S1

Correspondence to:
Y. Zhang,
yihuai.zhang@postgrad.curtin.edu.au

Citation:
Zhang, Y., M. Lebedev, M. Sarmadivaleh, A. Barifcani, and S. Iglauer (2016), Swelling-induced changes in coal microstructure due to supercritical CO_2 injection, *Geophys. Res. Lett.*, *43*, 9077–9083, doi:10.1002/2016GL070654.

Received 29 JUL 2016
Accepted 24 AUG 2016
Accepted article online 28 AUG 2016
Published online 14 SEP 2016

Swelling-induced changes in coal microstructure due to supercritical CO_2 injection

Yihuai Zhang[1], Maxim Lebedev[2], Mohammad Sarmadivaleh[1], Ahmed Barifcani[1], and Stefan Iglauer[1]

[1]Department of Petroleum Engineering, Curtin University, Kensington, Western Australia, Australia, [2]Department of Exploration Geophysics, Curtin University, Kensington, Western Australia, Australia

Abstract Enhanced coalbed methane recovery and CO_2 geostorage in coal seams are severely limited by permeability decrease caused by CO_2 injection and associated coal matrix swelling. Typically, it is assumed that matrix swelling leads to coal cleat closure, and as a consequence, permeability is reduced. However, this assumption has not yet been directly observed. Using a novel in situ reservoir condition X-ray microcomputed tomography flooding apparatus, for the first time we observed such microcleat closure induced by supercritical CO_2 flooding in situ. Furthermore, fracturing of the mineral phase (embedded in the coal) was observed; this fracturing was induced by the internal swelling stress. We conclude that coal permeability is drastically reduced by cleat closure, which again is caused by coal matrix swelling, which again is caused by flooding with supercritical CO_2.

1. Introduction

CO_2-enhanced coalbed methane (ECBM) recovery, especially in combination with carbon geosequestration in deep unmineable coal seams, has received considerable interest in recent years [e.g., *Shi and Durucan*, 2005a, 2005b; *Kaveh et al.*, 2011; *Chen et al.*, 2012; *Syed et al.*, 2013]. Technically, CO_2 is injected into the coal seams and it adsorbs onto the coal surface in micropores and fractures thereby displacing methane [*Zhang et al.*, 2011; *Moore*, 2012]. However, the coal matrix swells when CO_2 is injected [*Reucroft and Patel*, 1986; *Karacan*, 2003; *Izadi et al.*, 2011; *Wang et al.*, 2011], which drastically reduces the coal permeability by orders of magnitudes [*Pekot and Reeves*, 2003; *Shi and Durucan*, 2005b] and consequently seriously limits application of this technology [*Reeves*, 2004]. Mechanistically, it has been hypothesized that the dramatic permeability decrease is caused by cleat closure induced by coal swelling [*Mazumder et al.*, 2006; *Pan and Connell*, 2007; *Wu et al.*, 2011]. However, this effect has not been directly observed yet.

We thus imaged the changes in coal microstructure caused by supercritical (sc) CO_2 injection directly in situ via high-resolution X-ray microcomputed tomography at reservoir conditions, and we observed that the coal matrix swelled significantly due to CO_2 adsorption, which led to matrix cleat closure. Interestingly, new fractures were formed in the mineral phase by the internal swelling stresses in the coal matrix; however, the overall permeability drastically dropped.

2. Experimental Procedure

A small coal plug (diameter = 5 mm, length = 10 mm) was cut from a coal block acquired from 750 m depth at the Pingdingshan Ten coal mine, Henan, China. The coal was a typical subbituminous (medium rank) sample and had a carbon content of 54 (±2.0)% and a volatile matter content of 36 (±1.0)% measured by Chinese standard GB/T 212-2008. Nitrogen porosity and permeability (10.0% and 0.2 mD) were measured on a separate standard sister plug (38.1 mm diameter and 76 mm length) cut from the same block at 5 MPa effective stress (6 MPa confining pressure and 1 MPa injection pressure) with an AP-608 Permeameter-Porosimeter (accuracy ±0.1%).

The small cylindrical coal plug was then mounted into a high pressure-high temperature (HPHT) X-ray transparent core holder, which was integrated into a HPHT micro-CT (Xradia VersaXRM) core flooding apparatus (Figure 1) [cf. *Iglauer et al.*, 2011; *Rahman et al.*, 2016; *Zhang et al.*, 2016a, 2016b]. The swelling experiments were then conducted following below steps:

1. The core and tubing system were vacuumed for 24 h to ensure no air remained inside the system.

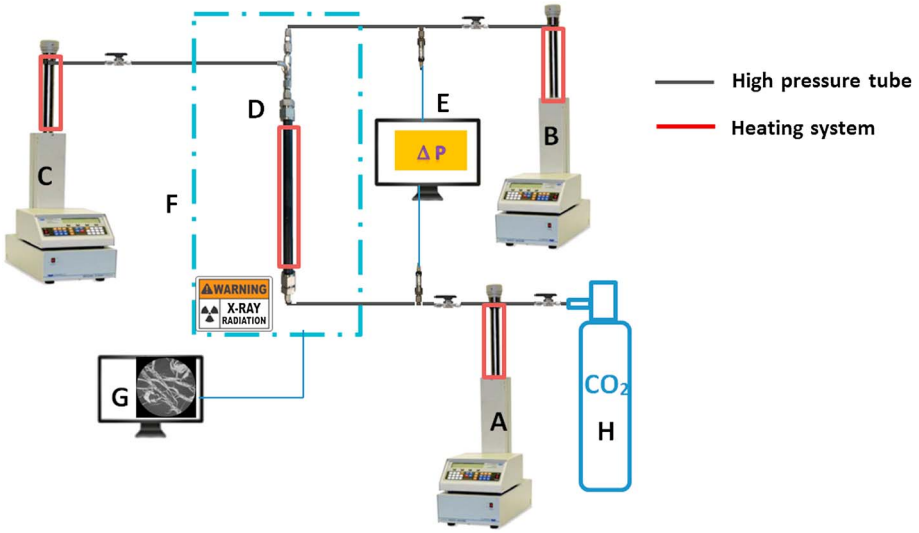

Figure 1. High pressure-high temperature in situ micro-CT core flooding apparatus: (A) injection pump, (B) production pump, (C) confining pressure pump, (D) core holder assembly, (E) pressure data acquisition, (F) micro-CT, (G) micro-CT image processing, and (H) CO_2 cylinder.

2. All flood lines, fluids, and the core holder were continuously isothermally heated to 323 K (=50°C) with heat jackets and continuously circulating warm water.
3. A confining pressure of 5 MPa (effective stress = 5 MPa) was applied, and the sample was imaged at a high resolution of 3.43 μm^3 in situ.
4. The coal plug was then flooded with supercritical CO_2 at 10 MPa backpressure, while a confining pressure of 15 MPa was applied (i.e., the experiment was conducted at constant effective stress; 5 MPa). The $scCO_2$ was injected at 0.1 mL/min flow rate (viscosity of the CO_2 was 0.0326 MPa s [*Fenghour et al.*, 1998]). The pressure drop across the coal plug was continuously measured with high-accuracy pressure sensors (Keller PAA-33X, accuracy 0.1%), and dynamic permeability was calculated via Darcy's law. Flooding was stopped after 17 h when more than 5000 pore volumes (PVs; note that 1 PV = 19.63 mm^3) of $scCO_2$ were injected.
5. The coal plug was then micro-CT imaged again at the same high resolution (3.43 μm^3) in situ at 323 K and 10 MPa pore pressure.
6. All micro-CT tomograms acquired were filtered with a 3-D nonlocal mean filter [*Buades et al.*, 2005] and segmented with a watershed algorithm [*Roerdink and Meijster*, 2000; *Schlüter et al.*, 2014] for the quantitative analysis.

3. Results and Discussion

3.1. Microcleat Morphology Changes and Associated Permeability Reduction

The microstructure of the coal is visualized in Figures 2 and 3, where microcleats are black, the mineral phase is white (the mineral phase was identified as $CaCO_3$ by scanning electron microscope–energy-dispersive X-ray spectroscopy analysis), and the coal matrix is dark grey (Figure 2) or illustrated in color in 3-D (coal matrix is blue, mineral phase is green, and microcleats are red; Figure 3). The volume fractions of these phases were then measured on the segmented images (71.4% coal matrix, 28.2% mineral phase, and 0.4% microcleats), and the morphologies of the microcleats were analyzed; width ~5–10 μm and lengths up to 2 mm were measured, with an effectively random distribution in the coal matrix. The microcleat volume percentage (0.4%) was much smaller when compared to the total porosity (10% nitrogen gas porosity (see above), including both cleat system and coal matrix; note that the pore structure in the matrix is nanoscale

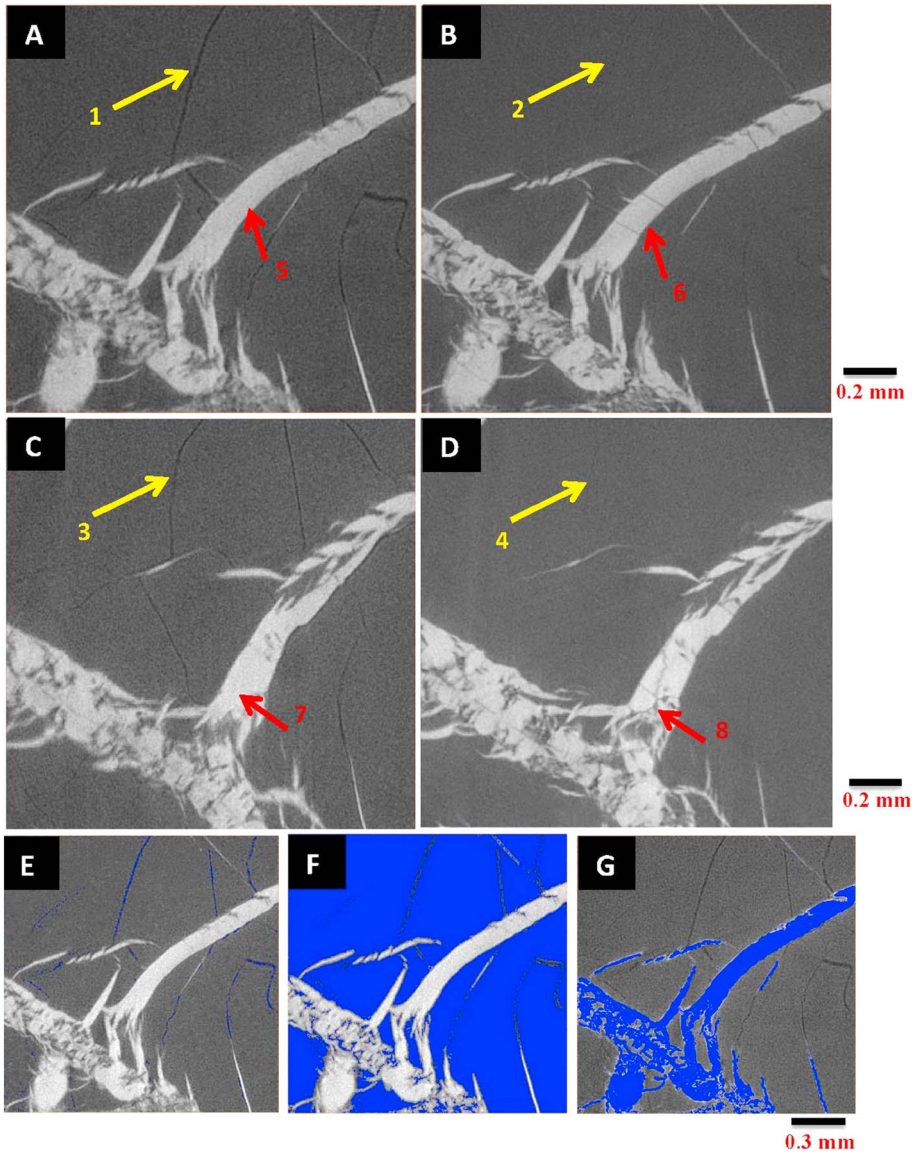

Figure 2. (A) Image slice through the coal before $scCO_2$ flooding (raw image); microcleats are black, coal matrix is dark grey, and mineral phase is white. (B) Image slice (same area as in Figure 2a) after $scCO_2$ injection (raw image); the cleats in the coal matrix disappeared (cf. points 1 and 2). Another example of coal matrix cleat closure (C) before and (D) after $scCO_2$ injection (cf. points 3 and 4). Furthermore, new fractures appeared in the mineral phase after $scCO_2$ flooding (cf. points 5 and 6 and 7 and 8). (E) Microcleats (blue), segmented image; (F) coal matrix (blue), segmented image; and (G) mineral phase (blue), segmented image.

[*Harpalani and Chen*, 1997; *Cui et al*., 2004], which cannot be resolved by micro-CT); however, the microcleats still controlled the permeability.

In this unconstrained condition (but at constant confining stress), the permeability rapidly and substantially decreased from 0.2 md to 0.002 md during $scCO_2$ flooding (Figure 4). Such a large permeability reduction is consistent with previous studies: *Reeves* [2004] observed a 1 order magnitude permeability reduction near the wellbore in a field experiment, and *Siriwardane et al*. [2009] measured a 90% permeability decrease in a lab test. Now when comparing the microcleat morphology (Figures 2 and 3) before and after $scCO_2$ flooding, a significant change is obvious. All cleats in the coal matrix closed, and as cleats are the major fluid conduits [*Laubach et al*., 1998], this observation is consistent with the independently measured drastic permeability drop.

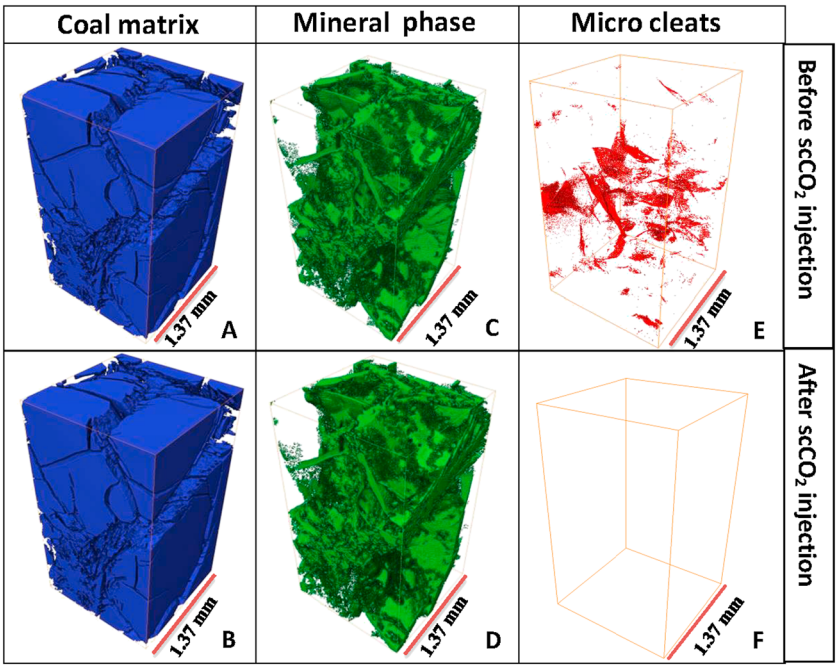

Figure 3. The 3-D visualization of coal matrix (blue), (A) before and (B) after $scCO_2$ injection. The 3-D visualization of mineral phase (green), (C) before and (D) after $scCO_2$ injection. The 3-D visualization of microcleats (red), (E) before and (F) after $scCO_2$ injection. The volumes shown are 5.16 mm^3 ($400 \times 400 \times 800$ voxels).

3.2. New Fractures Appeared in the Mineral Phase

Furthermore, we observed an interesting phenomenon: new fractures appeared in the mineral phase (Figures 2 and 5 and supporting information). These new fractures were mainly located at the interface between coal matrix and mineral phase. Their width was ~5 μm, and they usually spread through the whole width of the mineral vein (length $<$0.3 mm). Mechanistically, these new fractures were created by the coal matrix swelling stress (the swelling stress as hypothesized by *Liu and Rutqvist* [2010]). This becomes clear when measuring the volume matrix strains for the phases on the micro-CT images and applying the swelling stress (σ_s) theory. Based on this analysis (details are given in the supporting information), we calculated an internal swelling stress in the coal matrix of 15.52 MPa. Thus, the compressive stress exerted onto the mineral was above the plastic deformation limit of limestone (which for example is approximately 13 MPa for St. Maximin limestone [*Baud et al*., 2009]).

Furthermore, these newly formed fractures in the mineral phase were likely the cause of the residual permeability in the swollen coal (cf. Figure 4). Indeed, we observed a slight (but significant) pressure drop after ~8 h injection time (Figure 4), and we attribute this to the formation of a new fracture in the mineral phase. However, these new fractures were typically disconnected and much shorter when compared with the cleats in the coal matrix; moreover, the mineral phase was heterogeneously distributed in the coal matrix, and thus, permeability was not significantly influenced by these new fractures. Note that the porosity of the mineral phase (fractures' volume fraction) increased from 1.2% to 5.6% after $scCO_2$ injection (cf. also Figure 5). We also measured the size distribution of the fractures in the mineral phase (Figure 4); the number of small fractures (less than 1000 μm^3) decreased after $scCO_2$ injection, which is probably caused by internal swelling stress compression. However, the number of larger fractures ($>$1000 μm^3) increased, leading to an overall porosity increase in the mineral phase (see above).

4. Conclusions

Coal permeability is a key parameter, which determines the efficiency of CO_2-enhanced coalbed methane recovery and geological CO_2 sequestration in unmineable coal seams. However, a sharp drop in

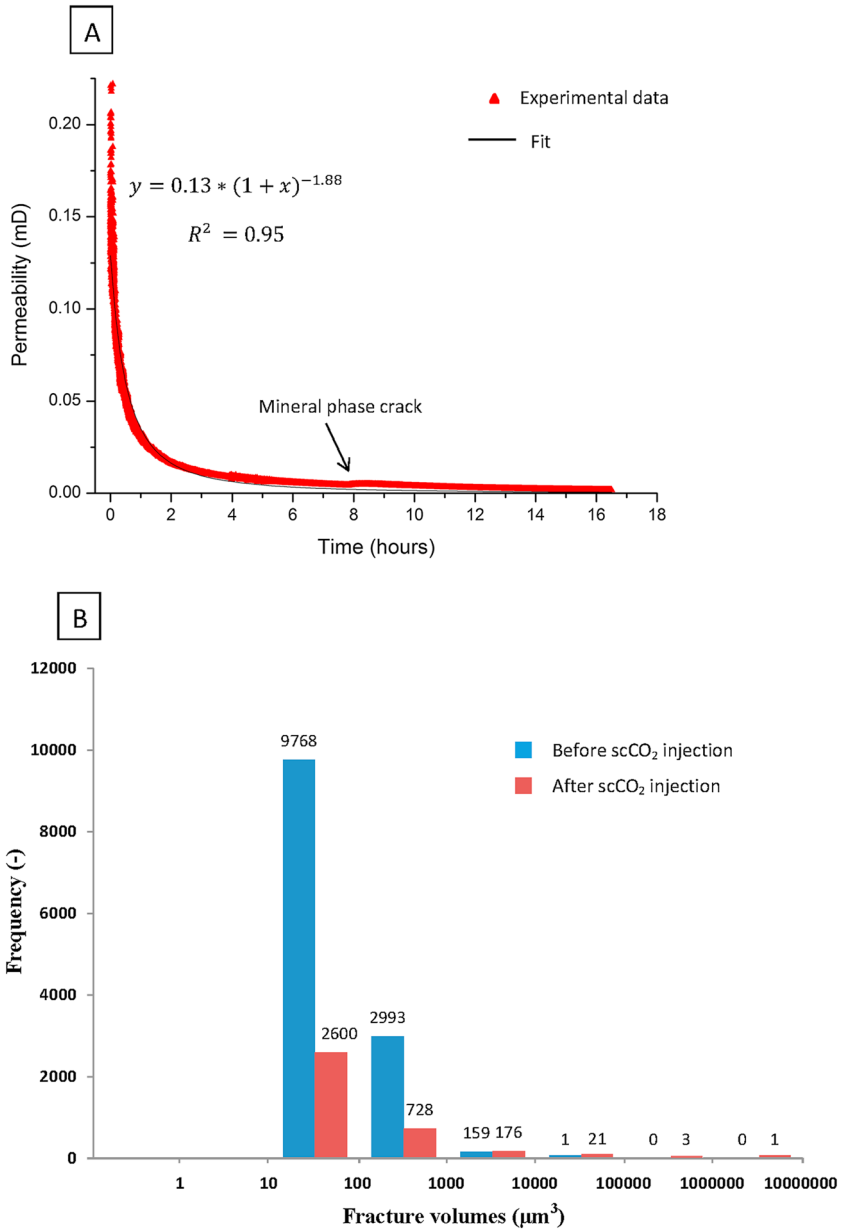

Figure 4. (A) Dynamic permeability measured injection time ($scCO_2$ was injected at 0.1 mL/min). (B) Fracture size distribution in mineral phase before and after $scCO_2$ injection.

permeability during the CO_2 injection process [*Shi and Durucan*, 2005b; *Larsen* 2004] severely limits application of this technology [*Reeves*, 2004]. Permeability is mainly determined by the cleat network and cleat morphology [*Harpalani and Chen*, 1992]; however, how CO_2 adsorption changes this cleat network is poorly understood.

We thus imaged a coal plug at reservoir conditions (15 MPa confining pressure, 5 MPa effective stress, and 323 K) before and after $scCO_2$ injection in situ with a novel HPHT micro-CT core flooding apparatus [*Iglauer et al.*, 2011; *Rahman et al.*, 2016], which can mimic near-injection wellbore conditions. We observed that all microcleats in the coal matrix were closed due to CO_2 adsorption, consistent with the dramatic decrease in permeability (from 0.2 mD to 0.002 mD). Interestingly, new fractures were formed in the mineral phase (carbonate) by internal swelling stress (porosity of the mineral phase increased from 1.2% to 5.6%).

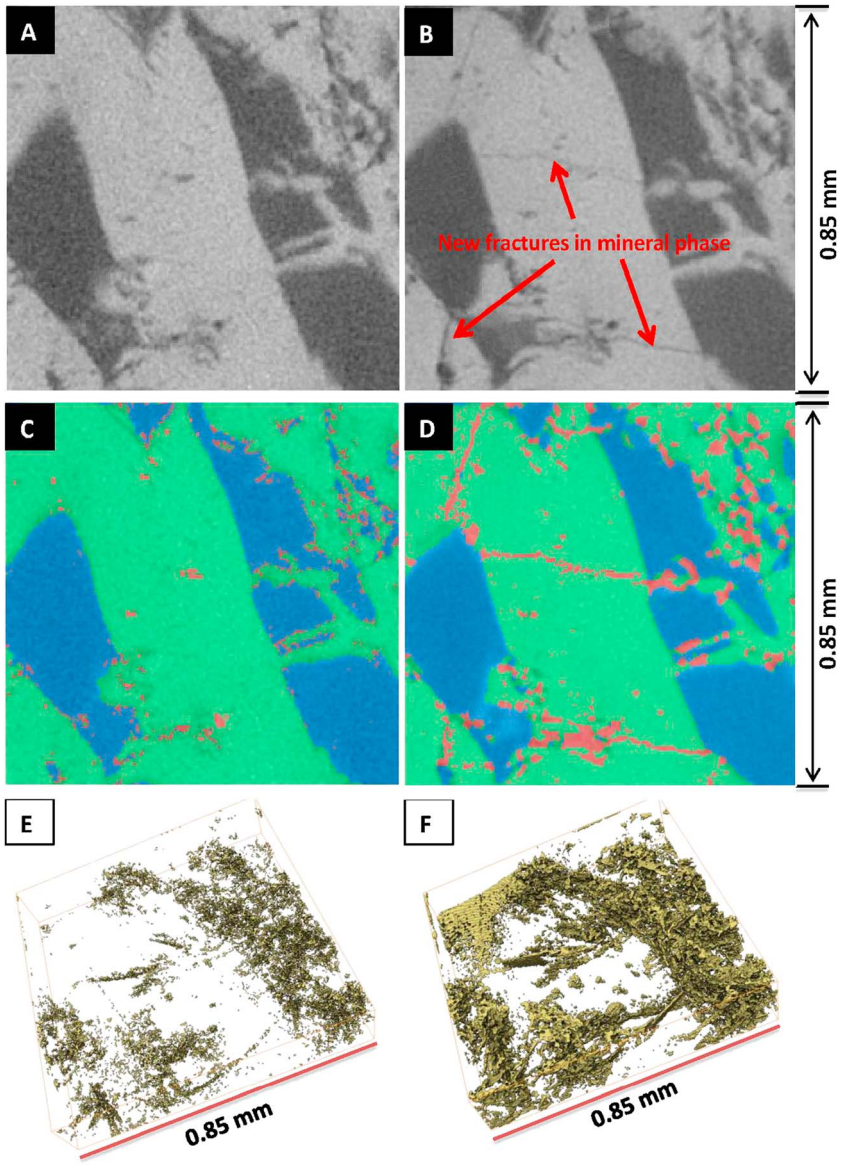

Figure 5. Image slices through coal plug: (A) before CO_2 injection (raw image); (B) after CO_2 injection (raw image); and (C and D) segmented images (Figures 5A and 5B) with fractures (red) in minerals, mineral (green), and coal matrix (blue). The 3-D visualization of fractures in the mineral phase (same area as in Figures 5a–5d), (E) before $scCO_2$ injection and (F) after $scCO_2$ injection. Figures 5E and 5F show a volume of ~0.12 mm^3 ($250 \times 250 \times 50$ voxels).

We conclude that coal matrix swelling due to CO_2 adsorption dramatically changes the morphology of the microcleat network and thereby drastically reduces coal permeability, and such swelling induces fracturing of the mineral phase in the coal seam.

Acknowledgments
The measurements were performed using the μCT system courtesy of the National Geosequestration Laboratory of Australia, funded by the Australian Federal Government.

References

Baud, P., S. Vinciguerra, C. David, A. Cavallo, E. Walker, and T. Reuschlé (2009), Compaction and failure in high porosity carbonates: Mechanical data and microstructural observations, in *Rock Physics and Natural Hazards*, pp. 869–898, Springer, New York.

Buades, A., B. Coll, and J.-M. Morel (2005), A non-local algorithm for image denoising, paper presented at Computer Vision and Pattern Recognition, 2005. CVPR 2005, IEEE Computer Society Conference on, IEEE.

Chen, Z., J. Liu, Z. Pan, L. D. Connell, and D. Elsworth (2012), Influence of the effective stress coefficient and sorption-induced strain on the evolution of coal permeability: Model development and analysis, *Int. J. Greenhouse Gas Control*, *8*, 101–110.

Cui, X., R. M. Bustin, and G. Dipple (2004), Selective transport of CO_2, CH_4, and N_2 in coals: Insights from modeling of experimental gas adsorption data, *Fuel*, *83*(3), 293–303.

Fenghour, A., W. A. Wakeham, and V. Vesovic (1998), The viscosity of carbon dioxide, *J. Phys. Chem. Ref. Data*, *27*(1), 31–44.
Harpalani, S., and G. Chen (1992), Effect of gas production on porosity and permeability of coal, paper presented at Proceedings of the Symposium of Coalbed Methane R and D in Australia.
Harpalani, S., and G. Chen (1997), Influence of gas production induced volumetric strain on permeability of coal, *Geotech. Geol. Eng.*, *15*(4), 303–325.
Iglauer, S., A. Paluszny, C. H. Pentland, and M. J. Blunt (2011), Residual CO_2 imaged with X-ray micro-tomography, *Geophys. Res. Lett.*, *38*, L21403, doi:10.1029/2011GL049680.
Izadi, G., S. Wang, D. Elsworth, J. Liu, Y. Wu, and D. Pone (2011), Permeability evolution of fluid-infiltrated coal containing discrete fractures, *Int. J. Coal Geol.*, *85*(2), 202–211.
Karacan, C. Ö. (2003), Heterogeneous sorption and swelling in a confined and stressed coal during CO_2 injection, *Energy Fuels*, *17*(6), 1595–1608.
Kaveh, N. S., E. S. J. Rudolph, K.-H. A. Wolf, and S. N. Ashrafizadeh (2011), Wettability determination by contact angle measurements: hvBb coal–water system with injection of synthetic flue gas and CO_2, *J. Colloid Interface Sci.*, *364*(1), 237–247.
Larsen, J. W. (2004), The effects of dissolved CO_2 on coal structure and properties, *Int. J. Coal Geol.*, *57*(1), 63–70.
Laubach, S., R. Marrett, J. Olson, and A. Scott (1998), Characteristics and origins of coal cleat: A review, *Int. J. Coal Geol.*, *35*(1), 175–207.
Liu, H.-H., and J. Rutqvist (2010), A new coal-permeability model: Internal swelling stress and fracture–matrix interaction, *Transp. Porous Media*, *82*(1), 157–171.
Mazumder, S., A. A. Karnik, and K.-H. A. Wolf (2006), Swelling of coal in response to CO_2 sequestration for ECBM and its effect on fracture permeability, *SPE J.*, *11*(03), 390–398.
Moore, T. A. (2012), Coalbed methane: A review, *Int. J. Coal Geol.*, *101*, 36–81.
Pan, Z., and L. D. Connell (2007), A theoretical model for gas adsorption-induced coal swelling, *Int. J. Coal Geol.*, *69*(4), 243–252.
Pekot, L., and S. Reeves (2003), Modeling the effects of matrix shrinkage and differential swelling on coalbed methane recovery and carbon sequestration, paper presented at Paper 0328, proc. 2003 International Coalbed Methane Symposium. Univ. of Ala., Citeseer.
Rahman, T., M. Lebedev, A. Barifcani, and S. Iglauer (2016), Residual trapping of supercritical CO_2 in oil-wet sandstone, *J. Colloid Interface Sci.*, *469*, 63–68.
Reeves, S. R. (2004), The Coal-Seq project: Key results from field, laboratory and modeling studies, paper presented at Proceedings of the 7th International Conference on Greenhouse Gas Control Technologies (GHGT-7), Citeseer.
Reucroft, P., and H. Patel (1986), Gas-induced swelling in coal, *Fuel*, *65*(6), 816–820.
Roerdink, J. B., and A. Meijster (2000), The watershed transform: Definitions, algorithms and parallelization strategies, *Fund. Inform.*, *41*(1, 2), 187–228.
Schlüter, S., A. Sheppard, K. Brown, and D. Wildenschild (2014), Image processing of multiphase images obtained via X-ray microtomography: A review, *Water Resour. Res.*, *50*, 3615–3639, doi:10.1002/2014WR015256.
Shi, J., and S. Durucan (2005b), CO_2 storage in deep unminable coal seams, *Oil Gas Sci. Tech.*, *60*(3), 547–558.
Shi, J.-Q., and S. Durucan (2005a), A model for changes in coalbed permeability during primary and enhanced methane recovery, *SPE Reservoir Eval. Eng.*, *8*(04), 291–299.
Siriwardane, H., I. Haljasmaa, R. McLendon, G. Irdi, Y. Soong, and G. Bromhal (2009), Influence of carbon dioxide on coal permeability determined by pressure transient methods, *Int. J. Coal Geol.*, *77*(1), 109–118.
Syed, A., S. Durucan, J.-Q. Shi, and A. Korre (2013), Flue gas injection for CO_2 storage and enhanced coalbed methane recovery: Mixed gas sorption and swelling characteristics of coals, *Energy Procedia*, *37*, 6738–6745.
Wang, S., D. Elsworth, and J. Liu (2011), Permeability evolution in fractured coal: The roles of fracture geometry and water content, *Int. J. Coal Geol.*, *87*(1), 13–25.
Wu, Y., J. Liu, D. Elsworth, H. Siriwardane, and X. Miao (2011), Evolution of coal permeability: Contribution of heterogeneous swelling processes, *Int. J. Coal Geol.*, *88*(2), 152–162.
Zhang, D., S. Li, Y. Cui, W. Song, and W. Lin (2011), Displacement behavior of methane adsorbed on coal by CO_2 injection, *Ind. Eng. Chem. Res.*, *50*(14), 8742–8749.
Zhang, Y., M. Lebedev, M. Sarmadivaleh, A. Barifcani, T. Rahman, and S. Iglauer (2016a), Swelling effect on coal micro structure and associated permeability reduction, *Fuel*, *182*, 568–576.
Zhang, Y., X. Xu, M. Lebedev, M. Sarmadivaleh, A. Barifcani, and S. Iglauer (2016b), Multi-scale x-ray computed tomography analysis of coal microstructure and permeability changes as a function of effective stress, *Int. J. Coal Geol.*, *165*, 149–156.